New Insights on the High-Temperature Nanostructure Evolution of SiOC and B-Doped SiBOC Polymer-Derived Glasses

Raquel Peña-Alonso,[†] Gino Mariotto,[‡] Christel Gervais,[§] Florence Babonneau,[§] and Gian Domenico Soraru*,[†]

Department of Materials Engineering and Industrial Technologies, University of Trento, Via Mesiano 77, 38050 Trento, Italy, Department of Physics, Science Faculty, University of Trento, Via Sommarive 14, 38050 Povo, Trento, Italy, and Laboratoire de Chimie de la Matiere Condensee, Universitè Pierre et Marie Curie, 4 place Jussieu CC 174, Paris Cedex 05, France

Received May 4, 2007. Revised Manuscript Received August 29, 2007

SiOC and SiBOC polymer-derived glasses show a complex nanostructure in which nanocrystalline β-SiC and sp^2 C coexists with nanoclusters of amorphous SiO_2 or $SiO_2-B_2O_3$ and with mixed silicon oxycarbide and boron oxycarbide units. The characterization of the nanostructure is performed with a multiple technique approach on SiOC and SiBOC glasses before and after HF etching. The acid attack dissolves the silica-based nanoclusters and allows indirect information on their size and amount to be obtained. By increasing the pyrolysis temperature from 1200 up to 1500 °C the oxide clusters grow in size and amount in both SiOC and SiBOC glasses. Compared to the B-free SiOC glass, SiBOC is more easily etched and develops higher porosity and larger pore size. Boron has also an important effect on the ordering of the sp^2 C phase: it leads to thicker sp^2 C nanocrystals. This effect is remarkable because it starts at low temperature (1500 °C) compared to the usual temperature, 1800 °C, reported in the literature for different forms of nanocrystalline carbon. Raman analysis of SiBOC glasses pyrolyzed at 1500 °C clearly shows the presence of the D′ band at 1617 cm^{-1}. From this experimental result it is postulated that B enters into the graphene layers forming BC_3 units. Finally, the shift toward lower wavenumbers of the Raman spectra recorded on SiOC and SiBOC glasses after etching seems to reveal a high compressive stress acting along the basal sp^2 C planes of the graphite nanocrystals.

1. Introduction

It is well-known that the pyrolysis in an inert atmosphere of siloxane polymers or hybrid silica gels leads to a new class of C-containing materials, named silicon oxycarbide glasses (SiCO).[1] They belong to the broader family of PDC (polymer derived ceramics) materials.[2]

The polymer route to ceramic materials is a low-temperature process which basically consists on the following steps: (i) melting or dissolving a preceramic polymer and shaping it into the desired form, (ii) cross-linking (thermally or with the use of a catalyst) to obtain a preceramic network, and (iii) pyrolysis in inert atmosphere to convert the preceramic network into the PDC material.[3] The final structure of the PDC is formed step by step during the pyrolysis,[4] through exchange and radical reactions, with evolution of low molecular weight species.[5] This process has a highly shaping flexibility that allows the fabrication of a many different components: bulks,[6−7] fibers,[8−9] films,[10] foams,[11] and MEMS.[12] Moreover, PDCs have shown unique properties, such as high-temperature stability,[13] creep,[14−15] and oxidation resistance.[16−17] Functional properties such as low dielectric constant,[18] photoluminescence,[19] and electrical conductivity[20−21] have also been reported.

* Corresponding author. E-mail: soraru@ing.unitn.it.
[†] Department of Materials Engineering and Industrial Technologies, University of Trento.
[‡] Department of Physics, Science Faculty, University of Trento.
[§] Universitè Pierre et Marie Curie.

(1) Renlund, G. M.; Prochaszka, S.; Doremus, R. H. *J. Mater. Res.* **1991**, *6*, 2719−2722.
(2) Raj, R.; Riedel, R.; Soraru, G. D. *J. Am. Ceram. Soc.* **2001**, *84* (10), 2158−2159.
(3) Riedel, R.; Mera, G.; Hauser, R.; Klonczynski, A. *J. Ceram. Soc. Jpn.* **2006**, *114* (6), 425−444.
(4) Sorarù, G. D.; Babonneau, F.; Mackenzie, J. D. *J. Mater. Sci.* **1990**, *25* (9), 3886−3893.
(5) Soraru, G. D.; Pederiva, L.; Latourneire, J.; Raj, R. *J. Am. Ceram. Soc.* **2002**, *85* (9), 2181−2187.
(6) Riedel, R.; Passing, G.; Schonfelder, H.; Brook, R. J. *Nature* **1992**, *355*, 714−717.
(7) (a) Sorarù, G. D.; Sglavo, V. M.; Vulcan, F.; Babonneau, F. *Mater. Res. Soc. Symp. Proc.* **1993**, *287*, 245−250. (b) Soraru, G. D.; Kleebe, H. J.; Ceccato, R.; Pederiva, L. *J. Europ. Ceram. Soc.* **2000**, *20* (14−15), 2509−2517.
(8) Yajima, S.; Hasegawa, Y.; Okamura, K.; Matsuzawa, T. *Nature* **1978**, *273*, 525.
(9) (a) Ishikawa, T.; Kohtoku, Y.; Kumagawa, K.; Yamamura, T.; Nagasawa, T. *Nature* **1998**, *391*, 773−775. (b) Soraru, G. D.; Mercadini, M.; Dal Macshio, R.; Taulelle, F.; Babonneau, F. *J. Am. Ceram. Soc.* **1993**, *76* (10), 2595−2600.
(10) Colombo, P.; Paulson, T. E.; Pantano, C. G. *J. Am. Ceram. Soc.* **1997**, *80* (9), 2333−2340.
(11) Colombo, P.; Hellmann, J. R. *Mater. Res. Innovations* **2002**, *6* (5−6), 260−272.
(12) Liew, L. A.; Zhang, W. G.; An, L. N.; Shah, S.; Luo, R. L.; Liu, Y. P.; Cross, T.; Dunn, M. L.; Bright, V.; Daily, J. W.; Raj, R.; Anseth, K. *Am. Ceram. Soc. Bull.* **2001**, *80* (5), 25−30.
(13) (a) Wang, Z.-C.; Aldinger, F.; and Riedel, R. *J. Am. Ceram. Soc.* **2001**, *84*, 2179−2183. (b) Soraru, G. D.; Suttor, D. *J. Sol-Gel Sci. Technol.* **1999**, *14* (1), 69−74.
(14) Riedel, R.; Ruswisch, L. M.; An, L. N.; Raj, R. *J. Am. Ceram. Soc.* **1998**, *81* (12), 3341−3344.
(15) Rouxel, T.; Soraru, G. D.; Vicens, J. *J. Am. Ceram. Soc.* **2001**, *84*, 1052−1058.
(16) Modena, S.; Soraru, G. D.; Blum, Y.; Raj, R. *J. Am. Ceram. Soc.* **2005**, *88* (2), 339−345.
(17) Chollon, G. *J. Eur. Ceram. Soc.* **2000**, *20*, 1959−1974.

10.1021/cm071203q CCC: $37.00
Published on Web 10/11/2007

The structure of silicon oxycarbide glasses has been the focus of many studies. The local chemistry around Si, C, and O atoms is well-known. At low pyrolysis temperatures (800−1000 °C), ^{29}Si solid-state NMR showed the presence of mixed silicon oxycarbide units, SiC_xO_{4-x}, $0 \leq x \leq 4$, in which silicon atoms share bonds with C and O atoms.[22] As reported by Mutin the percentage of the various Si sites follows a purely random distribution.[23] In the same temperature range, ^{13}C magic angle spinning (MAS) NMR analysis revealed that C atoms, besides forming Si−C bonds, are also present in aromatic carbon structures.[24] No long range order is present in SiCO glasses at 1000 °C. Increasing the annealing temperature above 1200 °C and up to 1500 °C usually results in the formation of nanocrystalline β-SiC, as revealed by X-ray diffraction (XRD) analysis[25] and high-resolution transmission electron microscopy observations.[26] The nucleation of silicon carbide is also observed by ^{29}Si MAS NMR: by increasing the temperature above 1000 °C a progressive consumption of mixed silicon oxycarbide units occurs and the glassy network phase separates into, mainly, SiC_4 and SiO_4 units. The SiO_4 tetrahedra form small silica clusters in agreement with small-angle X-ray scattering (SAXS) studies.[27]

Wilson et al.[28] have shown that silicon oxycarbide glasses can be etched by HF. HF etching of SiOC glasses removes silica, forms a porous structure, and allows, through the characterization of the material after attack, information on the size and the amount of the amorphous silica nanodomains to be obtained.[29] A structural model for the silica nanodomains in SiOC glasses has also been proposed by Saha et al.[30] According to this model, SiOC glass annealed at $T \geq 1200$ °C consists of a cellular structure of silica domains surrounded by domain walls. The domain walls consist of graphene layers and mixed silicon oxycarbide units, SiC_xO_{4-x}, $1 \leq x \leq 4$.

Recently, B addition to silicon oxycarbide glasses has been studied with the aim of a further improvement of their high-temperature stability. Indeed, the presence of B in the silicon oxycarbide network has been found to (i) increase the decomposition temperature above 1500 °C (ii) to reduce the tendency to silica crystallization and (iii) to increase the crystallization rate of SiC.[31,32]

This work reports a structural characterization, between 1200 and 1500 °C, of SiOC and SiBOC glasses before and after HF etching. It provides new information on (i) the effect of pyrolysis temperature on the structural evolution of silicon oxycarbide glasses, in particular with respect to the size and amount of the silica nanodomains, (ii) the role of B on the development of the nanostructure, and (iii) the structure of the free C phase.

2. Experimental Procedures

2.1. Gel Preparation. B-free and B-containing samples were prepared by the sol−gel method using methyltriethoxysilane (MTES) and boric acid, following a procedure described in refs 29 and 31. MTES was purchased from ABCR (Germany) and $B(OH)_3$ from Carlo Erba (Italy) and both reagents were used as received. In this way two gel samples were prepared with an atomic ratio B/Si = 0 (B-free samples) and B/Si = 0.2 (B-containing samples). B-free hybrid silica gel, precursor for SiOC glasses, was obtained hydrolyzing MTES with acidic water (pH = 1, HCl) using the ratio H_2O/Si = 3. The hydrolysis was performed at 70 °C for 15 min, and then an ammonia solution was added to promote condensation and gelation. The B-containing gel, precursor for SiBOC glasses, was prepared dissolving, in the silicon alkoxide, the proper amount of $B(OH)_3$ without any addition of water.[33] The solution was cast into test tubes and left open at room temperature for gelation. All gels were dried at 70 °C for at least 10 days.

2.2. Glass Preparation. SiOC and SiBOC glasses were obtained from gel fragments, with a pyrolysis process under flowing Ar (100 mL/min) at 5 °C/min up to 1200, 1400, and 1500 °C for 1 h.

2.3. Glass Etching. The etching process was performed on 0.5 g of 80−120 μm sieved oxycarbide powders using an HF (20 vol % in H_2O) solution. The etching of SiOC and SiBOC glasses was performed by stirring the powders for 9 h at room temperature. Then, the solutions were filtered, and the powders were rinsed with distilled water and dried at 110 °C.

2.4. Characterization Techniques. SiOC and SiBOC glasses were characterized before and after etching by chemical analysis, XRD, the nitrogen gas adsorption (BET method), and Raman and ^{29}Si and ^{11}B MAS NMR spectroscopies.

Chemical analysis was performed by the Service Central d'Analyze du CNRS, Vernaison, France. Si, C, B, and H were measured. O was estimated by difference to 100%.

X-ray diffractograms were collected on a Rigaku Dmax diffractometer in the Bragg−Brentano configuration using Cu Kα radiation, operating at 40 kV and 30 mA. A 2θ range of 10−80° was scanned with a step size of 0.05° and acquisition time of 5 s per point.

Nitrogen gas adsorption analyses were performed on the unetched and etched powders, but significant data were only obtained from the etched specimens as the unetched materials are full dense glasses. The isotherms were collected at 77 K using an ASAP 2010 (Micromeritics) instrument. The samples were previously degassed

(18) Valentinotti, M.; Walter, S.; Modena, S.; Sorarù, G. D. *J. Eur. Ceram. Soc*. **2007**, *27*, 2529−2533.
(19) (a) Soraru, G. D.; Modena, S.; Bettotti, P.; Das, G.; Mariotto, G.; Pavesi, L. *Appl. Phys. Lett*. **2003**, *83* (4), 749−751. (b) Sorarù, G. D.; Zhang, Y.; Ferrari, M.; Zampedri, L.; Goncalves, R. R. *J. Eur. Ceram. Soc*. **2005**, *25*, 277−281.
(20) Haluschka, C.; Engel, C.; Riedel, R. *J. Eur. Ceram. Soc*. **2000**, *20* (9), 1365−1374.
(21) Cordelair, J.; Greil, P. *J. Eur. Ceram. Soc*. **2000**, *20* (9), 1947−1957.
(22) Pantano, C. G.; Singh, A. K.; Zhang, H. *J. Sol-Gel Sci. Technol*. **1999**, *14*, 7−25.
(23) Mutin, P. H. *J. Am. Ceram. Soc*. **2002**, *85* (5), 1185−1189.
(24) Trimmel, G.; Badheka, R.; Babonneau, F.; Latournerie, J.; Dempsey, P.; Balhoul, D.; Parmentier, J.; Sorarù, G. D. *J. Sol-Gel Sci. Technol*. **2003**, *26*, 279−283.
(25) Bréquel, H.; Parmentier, J.; Walter, S.; Badheka, R.; Trimmel, G.; Masse, S.; Latournerie, J.; Dempsey, P.; Turquat, C.; Desmartin-Chomel, A.; Le Neindre-Prum, L.; Jayasooriya, U. A.; Hourlier, D.; Kleebe, H.-J.; Sorarù, G. D.; Enzo, S.; Babonneau, F. *Chem. Mater*. **2004**, *16*, 2585−2598.
(26) Turquat, C.; Kleebe, H. J.; Gregori, G.; Walter, S.; Sorarù, G. D. *J. Am. Ceram. Soc*. **2001**, *84* (10), 2189−2196.
(27) Lipowitz, J.; Rabe, J. A.; Frevel, L. K.; Miller, R. L. *J. Mater. Sci*. **1990**, *25*, 2118−2124.
(28) Wilson, M.; Zank, G.; Eguchi, K.; Xing, W.; Yates, B.; Dahn, J. R. *Chem. Mater*. **1997**, *9* (10), 2139−2144.
(29) Peña-Alonso, R.; Raj, R.; Soraru, G. D. *J. Am. Cearm. Soc*. **2006**, *89* (8), 2473−80.
(30) Saha, A.; Raj, R.; Williamson, D. L. *J. Am. Ceram. Soc*. **2006**, *89* (7), 2188−2195.
(31) Schiavon, M. A.; Gervais, C.; Babonneau, F.; Soraru, G. D. *J. Am. Ceram. Soc*. **2004**, *87*, 203−208.
(32) Klonczynski, A.; Schneider, G.; Riedel, R.; Theissmann, R. *Adv. Eng. Mater*. **2004**, *6*, 64−68.
(33) Soraru, G. D.; Babonneau, F.; Gervais, C.; Dallabona, N. *J. Sol-Gel Sci. Technol*. **2000**, *18*, 11−19.

Table 1. Chemical Composition of Selected SiOC and SiBOC Glasses before and after Etching[a]

	composition (wt %)					empirical formula[b,c] (EF)	
sample	Si	B	C	H	O	EF normalized on Si	EF normalized on C
SiOC	46.2		14.5	<0.3	39.3	$SiC_{0.73}O_{1.49}$	$Si_{1.37}C_1O_{2.04}$
SiBOC	41.0	3.2	11.8	<0.3	44.1	$SiB_{0.22}C_{0.67}O_{1.88}$	$Si_{1.49}B_{0.32}C_1O_{2.80}$
SiOC-HF	35.2		34.2	1.3	29.4	$SiC_{2.27}O_{0.96}$	$Si_{0.44}C_1O_{0.42}$
SiBOC-HF	26.3	1.8	33.0	1.7	37.2	$SiB_{0.19}C_{2.93}O_{1.57}$	$Si_{0.34}B_{0.06}C_1O_{0.54}$

[a] Glasses have been pyrolyzed at 1400 °C for 1 h. Oxygen Was estimated by difference to 100%. Empirical formulas are normalized on Si and on C. [b] For the un-etched samples, H has been found below the detectable limit and is not reported in the EF. [c] For the ectched samples, the chemical analysis revealed a certain amount of hydrogen arising from the water retained in the porous structure from the etching process. The EFs of the etched oxycarbide samples have been obtained by deducting the water molecules corresponding to the hydrogen content following a procedure reported in ref 29.

at 200 °C for at least 4 h before analysis. Specific surface area (SSA) was determined from a BET (Brunauer, Emmet, and Teller)[34] analysis in the P/P_0 range of 0.05−0.30 using a molecular cross-sectional area for N_2 of 0.163 nm^2 and a minimum of five data points. The pore size distributions (PSDs) were obtained from the adsorption branch of the isotherm through the BJH (Barret, Joyner, and Halenda) analysis.[35] The mesopore volume represented the cumulative volume of the pores with radii ranging from 2 to 50 nm, and the average pore diameter has been obtained from $4V/A$, where V is the volume and A is the surface area of the mesopores.

The Raman spectra were collected on a Jobin Yvon Raman spectrometer, model Olympus BX41 (Horiba) with an excitation wavelength of 632.817 nm (He−Ne laser) and using a CCD detector and a ×100 objective with NA = 0.9.

^{11}B and ^{29}Si MAS NMR spectra were recorded at 128.28 and 75.49 MHz (model AVANCE, Bruker Instruments, Karlsruhe, Germany). The ^{29}Si spectra were recorded using a CP MAS probe (model MAS, Bruker Instruments) equipped with 7 mm ZrO_2 rotors, spinning at 4 kHz. The following parameters were used: spectral width of 30 kHz, 4000 data points, pulse width of 2 μs ($\theta \approx 30°$), and recycle delays of 60 s. Spectra were referenced externally to tetramethylsilane (TMS) at 0 ppm. The ^{11}B NMR spectra were recorded using a cross-polarization (CP) MAS (Doty Scientific, Columbia, SC) probe equipped with 5 mm Si_3N_4 rotors, spinning at 9 kHz. Spectral width was 125 kHz, 4000 data points, pulse width of 1 μs ($\theta \approx 15°$), and recycle delay of 1 s. Spectra were referenced externally to $BF_3(OEt)_2$ at 0 ppm. The spectra were simulated with the DMFIT program.[36]

3. Experimental Results

3.1. Characterization of SiOC and SiBOC Glasses (before Etching). *3.1.1. Chemical Analysis.* A study of the chemical modification of SiOC and SiBOC glasses pyrolyzed at various temperatures in the range 1000−1500 °C has been already reported in the literature and showed that these glasses are thermally stable (weight loss at 1500 °C ≤ 1 wt %) and that their chemical composition is constant in this temperature range.[31] Accordingly, in the present study, the chemical analysis, CA, has been performed only on the SiOC and SiBOC samples pyrolyzed at 1400 °C for 1 h and gave the following results (wt %): Si = 46.2; C = 14.5; H < 0.3; and O = 39.3 for SiCO and Si = 41.0; B = 3.2; C = 11.8; H < 0.3; and O = 44.1 for SiBOC (Table 1). The corresponding chemical formulas are $SiC_{0.73}O_{1.49}H_{<0.18}$ and $SiB_{0.22}C_{0.67}O_{1.87}H_{<0.18}$ for SiCO and SiBOC respectively. The B content was found close to the theoretical value (B/Si = 0.2). The C content is similar for the two glasses, and the results are in agreement with those previously reported for analogous samples.[31]

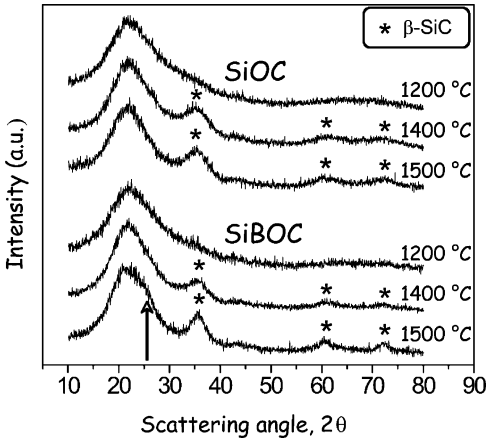

Figure 1. XRD pattern of SiOC and SiBOC materials pyrolyzed at different temperatures for 1 h. The arrow points to the shoulder in the spectrum of the SiBOC glass annealed at 1500 °C assigned to the (002) reflection of graphitic carbon.

3.1.2. XRD Study. XRD patterns collected on SiOC and SiBOC samples pyrolyzed at 1200, 1400, and 1500 °C for 1 h are shown in Figure 1. The spectrum of the SiOC and SiBOC samples pyrolyzed at 1200 °C show a completely amorphous structure with only the presence of the silica halo centered at about $2\theta = 22°$. The increase of the pyrolysis temperature promotes the crystallization of β-SiC. The (111) diffraction peak of cubic SiC at $2\theta \approx 35°$ and the related reflections at $2\theta \approx 60°$ (101) and 72° (211) start to appear in both samples at 1400 °C and become more evident at 1500 °C. In the XRD spectrum of SiBOC at 1500 °C is also evident a shoulder (indicated by the arrow in Figure 1) at $2\theta \approx 26.6°$ which can be attributed to the (002) reflection of graphitic carbon.[37] The analysis of the line broadening, according to the Scherrer equation, has been performed on the (111) peak of SiC and allows us to estimate the crystal size of β-SiC, $D_{SiC(111)}$ (Table 2). The data show that (i) the β-SiC nanocrystals grow with the pyrolysis temperature and (ii) the presence of B in the SiBOC samples promotes this process leading to slightly larger nanocrystals. These results are in complete agreement with our previous findings[31] and those reported by Klonczynski et al.[32]

3.1.3. Raman Study. The first-order Raman spectra for the SiOC and SiBOC materials pyrolyzed at 1400 and 1500 °C

(34) Gregg, S. J.; Sing, K. S. W. *Adsorption, Surface Area and Porosity*; Academic Press: London, 1982; pp 285−286.
(35) Barret, E. P.; Joyner, L. G.; Halenda, P. H. *J. Am Chem. Soc*. **1951**, *53*, 373−380.
(36) Massiot, D.; Fayon, F.; Capron, M.; King, I.; Le Calvé, S.; Alonso, B.; Durand, J. O.; Bujoli, B.; Gan, Z.; Hoatson, G. *Magn. Res. Chem*. **2002**, *40*, 70−76.
(37) JPCD 26-1080.

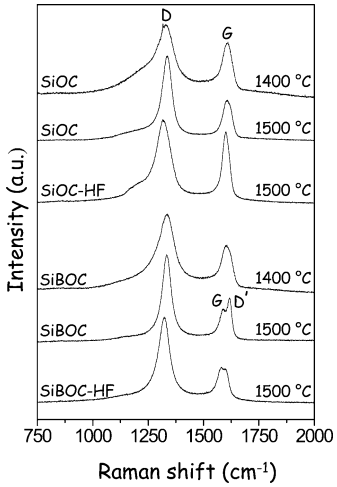

Figure 2. Raman spectra of SiOC and SiBOC glasses pyrolyzed for 1 h at 1400 (before etching) and 1500 °C (before and after etching).

Table 2. Crystallite Size, $D_{SiC(111)}$, of β-SiC Crystals and $L_{C(002)}$ of Nanocrystalline Graphite for Samples Pyrolyzed at 1400 and 1500 °C for 1 h before and after Being HF-Etched

	$D_{SiC(111)}$ (nm)		$L_{C(002)}$ (nm)
sample	1400 °C, 1 h	1500 °C, 1 h	1500 °C, 1 h
SiCO	2.6 ± 0.2	3.5 ± 0.2	
SiBOC	2.8 ± 0.2	3.7 ± 0.2	
SiCO-HF	2.7 ± 0.2	3.6 ± 0.2	2.9 ± 0.2
SiBOC-HF	2.9 ± 0.2	4.8 ± 0.2	5.3 ± 0.2

for 1 h are reported in Figure 2. The figure shows only the spectral region between 800 and 2000 cm^{-1}, where Raman scattering from boroxyl groups, from SiC, and from different carbon forms is expected to occur. No appreciable Raman scattering from both SiOC and SiBOC materials, even at the early steps of the pyrolysis process, was observed in the spectral region below 800 cm^{-1}, where the scattering from silicon oxide occurs, and therefore this spectral region is not shown in Figure 2. The lack of any appreciable spectral signature from the silicon oxide matrix is likewise due to its scarce Raman scattering cross section. The spectra collected at 1200 °C are dominated by a strong luminescent background and are omitted. The spectra in Figure 2 show the two characteristic features of disordered graphitic forms of carbon:[38] the D (disordered) band at around 1350 cm^{-1} and the G (graphite) band at around 1600 cm^{-1}. In contrast, no trace of the Raman signal from the SiC component can be observed, probably because of both the relatively low efficiency of SiC material and the reduced size of formed SiC nanocrystals. The higher energy G band is assigned to graphite single crystals, and it is caused by the vibrational mode (*E*2*g* symmetry in the *D*46*h* space group) of graphitic layers. The D band is observed in amorphous or nanocrystalline graphitic carbon, and it is usually related to the disorder associated with the finite crystallite size.[39,40] The Raman spectral parameters of the studied samples are reported in Table 3.

At 1400 °C both the oxycarbides show Raman spectra with the same spectral features in terms of peaks position and broadness. The G band is located around 1604−1608 cm^{-1}, and the D band at 1330−1335 cm^{-1}. Similar Raman spectra have been reported in the literature for gel-derived silicon oxycarbide glasses.[41,42] The almost complete superimposition of the two spectra (SiOC and SiBOC at 1400 °C) indicates that the structure of the carbon phase in these two samples are very similar. The type of disordered carbon in these materials, amorphous versus nanocrystalline, can be figured out from the position of the G band. Values close to 1600 cm^{-1} suggest the occurrence of a nanocrystalline form of graphite more than amorphous carbon. The difference between these two materials is essentially the presence, in the amorphous C, of a considerable amount of sp^3 C atoms (up to 20 atom %). This structural modification, that is, the presence in the graphene planes of sp^3 C atoms, leads to a continuous shift of the G peak from 1600 cm^{-1} toward lower frequencies, down to 1510 cm^{-1}.[38]

At 1500 °C the Raman spectrum of the B-free SiCO shows the two bands in the same position with the only difference being a narrowing of the D band (fwhm from 87 to 52 cm^{-1}). This evolution suggests a substantial stability, compared to 1400 °C, of the carbon structure with a slight ordering of the C nanocrystals, in agreement with the results reported by several authors on SiCO[41] and SiCN[43] PDC.

Conversely, the 1500 °C spectrum of the SiBOC samples reveals important changes of the 1600 cm^{-1} peak. The G band narrows and shifts to lower wavenumber (1590 cm^{-1}) toward the typical value for graphite, 1582 cm^{-1}. At the same time, a new peak, more intense than the G band, clearly emerges at 1617 cm^{-1}. This evolution suggests that, for SiBOC glass, a significant ordering of the graphite nanocrystals takes place from 1400 to 1500 °C. The new band, centered at about 1617 cm^{-1}, can be attributed to the D′ mode of the graphite.[38] The clear presence of the D′ band in silicon oxycarbide glasses or in Si-based PDC is reported here by the first time. The D′ band is found in nanocrystalline graphite and it is generally ascribed to a breakdown of the $K = 0$ selection rules by a local distortion of the graphite lattice due to the finite dimension of the nanocrystals.[38] However, the D′ band is also found to be more defined and intense in B-doped carbon.[44−45] The enhancement of the D′ band in B-doped carbons has been attributed to the partial substitution, in the graphene layers, of C with B atoms which acts as defects of the crystalline structure and reduces the in-plane correlation, thereby increasing the intensity of both the D and the D′ bands.[44]

3.2. Characterization of SiOC and SiBOC Glasses (after Etching). *3.2.1. Chemical Analysis.* The chemical

(38) Ferrari, A. C.; Robertson, J. *Phys. Rev. B* **2000**, *61* (20), 14095−14107.
(39) Wang, Y.; Alsmeyer, D. C.; McCreery, R. L. *Chem. Mater.* **1990**, *2*, 557−563.
(40) Dillon, R. O.; Woollam, J. A.; Katkanant, V. *Phys. Rev. B* **1984**, *29* (6), 3482−3489.
(41) Chomel, A. D.; Dempsey, P.; Latournerie, J.; Hourlier-Bahloul, D.; Jayasooriya, U. A. *Chem. Mater.* **2005**, *17*, 4468−4473.
(42) Sorarù, G. D.; D'Andrea, G.; Campostrini, R.; Babonneau, F.; Mariotto, G. *J. Am. Ceram. Soc.* **1995**, *78*, 379−387.
(43) Trassl, S.; Motz, G.; Rössler, E.; Ziegler, G. *J. Am. Ceram. Soc.* **2002**, *85* (1), 239−244.
(44) Endo, M.; Kim, C.; Karaki, T.; Tamaki, T.; Nishimura, Y.; Matthews, M. J.; Brown, S. D. M.; Dresselhaus, M. S. *Phys. Rev. B* **1998**, *58* (14), 8991−8996.
(45) Kim, C.; Fujino, T.; Hayashi, T.; Endo, M.; Dresselhaus, M. S. *J. Electrochem. Soc.* **2000**, *147* (4), 1265−1270.

Table 3. Peak Frequency (ω) and fwhm for the Raman D, G, and D′ Bands Observed in the Spectra of the SiCO and SiBOC Samples Pyrolyzed for 1 h at 1400 (before Etching) and 1500 °C (before and after Etching)

sample	pyrolysis parameters	ω_D (cm^{-1})	fwhm (cm^{-1})	ω_G (cm^{-1})	fwhm (cm^{-1})	$\omega_{D'}$ (cm^{-1})	fwhm (cm^{-1})
SiCO	1400 °C, 1 h	1330 ± 1	87 ± 2	1608 ± 1	54 ± 2		
	1500 °C, 1 h	1335 ± 1	52 ± 2	1610 ± 1	48 ± 2		
SiCO-HF	1500 °C, 1 h	1319 ± 1	74 ± 2	1601 ± 1	36 ± 2		
SiBOC	1400 °C, 1 h	1335 ± 1	82 ± 2	1604 ± 1	52 ± 2		
	1500 °C, 1 h	1335 ± 1	42 ± 2	1590 ± 1	33 ± 2	1617 ± 1	24 ± 2
SiBOC-HF	1500 °C, 1 h	1323 ± 1	70 ± 2	1582 ± 1	30 ± 2	1600 ± 1	25 ± 2

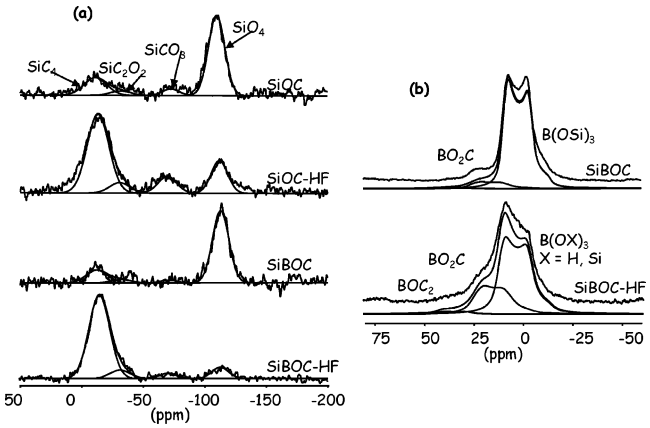

Figure 3. (a) ^{29}Si and (b) ^{11}B MAS NMR spectra collected on SiBOC samples pyrolyzed at 1400 °C for 1 h before and after being etched.

composition of the SiOC and SiBOC samples after etching is reported in Table 1 and compared with that of the un-etched glasses. It is known that etching silicon oxycarbide glasses by HF removes only silica[29] and that Si atoms bonded to C atoms via Si−C bonds are un-affected by this chemical treatment.[46] Then, the chemical composition of our samples before and after etching can be rewritten by normalizing it to C. Accordingly, it is straightforward to recognize the Si, B, and O depletions associated to the chemical attack. In the case of SiBOC, B and Si atoms are leach out with a B/Si atomic ratio of 0.23, which is quite close to the overall B/Si ratio present in the starting SiBOC glass (B/Si = 0.22).

3.2.2. ^{29}Si and ^{11}B MAS NMR. Useful information on the etching process can be obtained from the ^{29}Si and ^{11}B MAS NMR investigation of the SiOC and SiBOC samples after HF attack. The NMR spectra of samples pyrolyzed at 1400 °C for 1 h are reported in Figure 3 and compared with the same spectra recorded before etching. In the un-etched SiOC sample the ^{29}Si spectrum reveals a major component at −112 ppm (69%) due to silicon atoms in SiO_4 sites and the well-known formation of the mixed silicon oxycarbide units:[22,42] SiO_3C at −71 ppm (6%), SiO_2C_2 at −32 ppm (4%), and SiC_4 at −13 ppm (21%). SiC_3O units, expected around −1 ppm, cannot be excluded but would be present in very small amounts. The corresponding ^{29}Si spectra recorded on the SiBOC glass shows a similar pattern; however, in this case, mixed SiO_3C and SiO_2C_2 units are almost absent, and the network is more phase separated into SiO_4 and SiC_4 sites in agreement with the known effect of boron in promoting the phase separation of the silicon oxycarbide network into SiO_4 and SiC_4 sites.[31] The ^{11}B MAS NMR spectrum (Figure 3b) shows the presence of three components with similar quadrupolar parameters (CQ = 2.6 MHz and 0.2, where CQ is the quadrupolar coupling constant and the second value is the asymmetry parameter) characteristic of trigonal boron atoms. According to Gervais et al.,[47] the boron components can be attributed to the formation of the following sites: BO_3 at 12.5 ppm (93%), BO_2C at 29 ppm (7%), and BOC_2 at 46 ppm (1%). It can be noticed that the presence of the small amount of BOC_2 units is more obvious after etching. More precisely, the first peak at 12.5 ppm is actually indicative of trigonal B connected to SiO_4 tetrahedra, $B(OSi)_3$ in a borosilicate network,[48] while the two other ones are associated with BO_2C and BOC_2 mixed boron oxycarbide sites in which the boron atoms share bonds with oxygen and carbon atoms.[47] The small amount of BO_2C and BOC_2 units compared to $B(OSi)_3$ indicates that the boron is predominantly present in the silica-rich phase.

After etching, the ^{29}Si spectra (Figure 3 a) reveal, in both SiOC and SiBOC samples, a great decrease of the peak associated to SiO_4 sites (which is more pronounced for the SiBOC glass) and a corresponding increase of the silicon oxycarbide units, SiO_3C, SiO_2C_2, and SiC_4, in which silicon atoms share at least one bond with carbon atoms. The results of the quantitative analysis obtained by deconvoluting the experimental spectra are reported in Table 4.

Assuming that all SiC_xO_{4-x} ($x \neq 0$) units are maintained after etching, ^{29}Si NMR indicates that HF attack removes 2/3 of the initial SiO_4 units for SiCO and 3/4 for SiBOC, in good agreement with the chemical analysis (Table 1).

The ^{11}B NMR spectrum of the etched SiBOC glass shows an evolution similar to the ^{29}Si spectrum: the relative amount of the boron oxycarbide units, BO_2C and BOC_2, strongly increases compared to the BO_3 sites. Moreover, the BO_3 signal shows a shift to 15.4 ppm and therefore cannot be unequivocally associated to borosiloxane units, $B(OSi)_3$, but is more precisely assigned to $B(OX)_3$ with X = H, Si, that is, to BO_3 units in which oxygen atoms can bond either hydrogen or silicon atoms. Indeed, the ^{1}H MAS NMR spectrum recorded on the sample after etching clearly shows the presence of OH groups.

Assuming that all BO_2C and BOC_2 units are maintained after etching, ^{11}B NMR indicates that HF dissolves 4/5 of the inital of BO_3 units. Again, this result is in good agreement with the chemical analysis (Table 1).

^{29}Si and ^{11}B MAS NMR spectra have been also recorded for the SiBOC samples pyrolyzed at 1500 °C before and after HF etching. They are similar to the spectra obtained at

(46) Soraru, G. D.; Modena, S.; Guadagnino, E.; Colombo, P.; Egan, J.; Pantano, C. *J. Am. Ceram. Soc.* **2002**, *85* (6), 1529−1536.

(47) Gervais, C.; Babonneau, F.; Dallabona, N.; Soraru, G. D. *J. Am. Ceram. Soc.* **2001**, *84* (10), 2160−2164.

(48) van Wüllen, L.; Müller-Warmuth, W. *Solid State Nucl. Magn. Reson.* **1993**, *2*, 279.

Table 4. (a) ^{29}Si and (b) ^{11}B MAS NMR Characterization of SiOC and SiBOC Samples Pyrolyzed at 1400 °C for 1 h before and after Being HF-Etched[a]

(a)

	signal intensity (±1%)				molar amount		
	−112;[b] SiO_4[c]	−71;[b] $SiCO_3$[c]	−32;[b] SiC_2O_2[c]	−13;[b] SiC_4[c]	SiC_xO_{4-x} ($x \neq 0$)	SiO_4	*n*Si tot
SiOC	69	6	4	21	0.31	0.69	1
SiOC-HF	19	11	8	62	0.31	0.07	0.38
SiBOC	75	2	4	19	0.25	0.75	1
SiBOC−HF	8	4	8	80	0.25	0.02	0.27

(b)

	signal intensity (±1%)				molar amount			
	$B(OSi)_3$;[d] $\delta(^{11}B) = 12.6$ ppm; CQ = 2.6 MHz; $\eta = 0.2$	$B(OX)_3$[d] (X = Si, H); $\delta = 15.4$ ppm; CQ = 2.8 MHz; $\eta = 0.2$	BO_2C;[d] $\delta = 29.0$ ppm; CQ = 2.9 MHz; $\eta = 0.3$	BO_2C;[d] $\delta = 46.0$ ppm; CQ = 2.9 MHz; $\eta = 0.3$	BOC_2	BO_2C	BO_3	*n*B tot
SiBOC	92		7	1	0.01	0.07	0.92	1
SiBOC-HF		67	29	4	0.01	0.07	0.16	0.24

[a] The Loss of SiO_4 and BO_3 Units (for an initial normalized amount of Si and B) is calculated assuming that the amount of SiC_xO_{4-x} ($x \neq 0$) BO_2C and BOC_2 is maintained after etching. [b] δ_{iso} (^{29}Si; ppm). [c] Assignment. [d] Site.

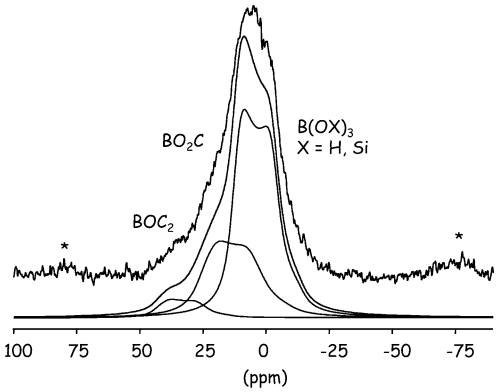

Figure 4. ^{11}B MAS NMR spectrum collected on SiBOC samples pyrolyzed at 1500 °C for 1 h after HF etching. * indicates spinning sidebands.

1400 °C: indeed, they show the presence of the same mixed Si and B sites (revealed at 1400 °C) in comparable amounts. The only slight difference was in the ^{11}B MAS NMR spectrum (Figure 4) after etching, which reveals the presence of a larger amount of B−C bonds (BOC_2 and BO_2C units). The percentages of the various B sites in this sample (SiBOC, 1500 °C, 1 h, HF etched) are BO_3, 63%; BO_2C, 31%; and BOC_2, 6%.

Thus, the NMR study clearly indicates that HF etching of SiOC and SiBOC glasses leads to a dissolution of the oxide-based phase with a loss of SiO_4 and BO_3 units. As previously reported, the chemical analysis reveals that the composition of the etched borosilicate phase has a B/Si atomic ratio equal to 0.23, that is, close to the overall glass composition (B/Si = 0.20) and corresponding to a borosilicate glass with molar composition SiO_2 nB_2O_3 with $n = 1.29$. Covalent Si−C and B−C bonds present in the starting glass seem stable against HF; they are not cleaved, and they are left behind in the solid residue.

3.2.3. N_2 Adsorption Analysis. All the "as-pyrolyzed" oxycarbide glasses are fully dense materials with a negligible SSA. The etching process, by removing SiO_2 from SiOC and the $SiO_2-B_2O_3$ borosilicate glass from SiBOC, creates a highly porous C-rich material. The porous residue was characterized by performing N_2 adsorption analyses, which gave the results reported in Table 5.

Table 5. SSA, Mesopore, and Micropore Volumes, and Average Pore Size for SiOC and SiBOC Etched Glasses

sample	pyrolysis parameters	SSA (m^2/g) ± 1%	mesopore volume (cm^3/g)[b]	micropore volume (cm^3/g)[c]	average pore size (nm)[b]
SiOC-HF	1200 °C, 1 h	204	0.10 ± 0.01	0.11 ± 0.01	2.1 ± 0.1
SiOC-HF	1400 °C, 1 h	482	0.14 ± 0.01	0.26 ± 0.01	2.6 ± 0.1
SiOC-HF	1500 °C, 1 h	562	0.23 ± 0.01	0.33 ± 0.01	2.8 ± 0.1
SiBOC-HF	1200 °C, 1 h				
SiBOC-HF	1400 °C, 1 h	567	0.12 ± 0.01	0.30 ± 0.01	2.8 ± 0.1
SiBOC-HF	1500 °C, 1 h	539	0.66 ± 0.01	0.54 ± 0.01	4.8 ± 0.1

[a] Mesopore range = 2−100 nm. Micropore range < 2 nm. [b] As obtained from the BJH mesopore distribution using the adsorption data of the isotherm. [c] Calculated from the *t*-plot analysis.

For both compositions the pore volume and the average pore size increases with the pyrolysis temperature. The surface area increases for the SiOC composition while, for the B-containing samples, the SSA measured at 1500 °C (539 m^2/g) is slightly lower than that at 1400 °C (567 m^2/g). Because the characterization of the pores present in the etched materials represents the negative picture of the unetched glasses, these results indicate that the amount and the size of the oxide-based phase which can be leached out increases with the pyrolysis temperature. Interestingly, the SiBOC glasses at 1200 °C cannot be etched: the SSA and pore volume are still negligible after HF attack. (The reason for this result will become clear in the Discussion section.)

By comparing the data of SiOC and SiBOC at 1400 °C and 1500 °C, we can see that SiBOC glasses develop more porosity and larger pore sizes than the B-free SiOC. Nitrogen adsorption isotherms and PSD curves obtained on the SiOC and SiBOC samples pyrolyzed at 1500 °C for 1 h are shown in Figure 5. Both isotherms for the adsorbed volume rise rapidly at very low values of the relative pressure. This steep rise arises from the micropores (diameter below 2 nm). On the other hand, a strong difference exists between the two samples in the mesoporous range. The large hysteresis loop seen for the SiBOC glass is absent for the SiOC composition and accounts for the large amount of mesopores observed for the B-containing samples ($V_{mesopores} = 0.66$ cm^3/g and 0.23 cm^3/g for SiBOC and SiOC, respectively). The PSD curves very clearly indicate that for SiOC the pore size is

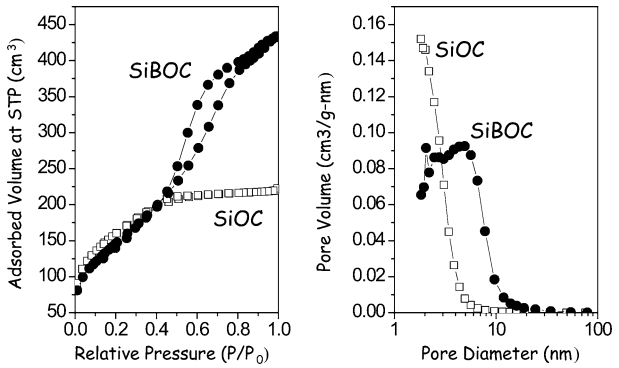

Figure 5. (a) Nitrogen adsorption isotherms and (b) PSD curves for SiOC and SiBOC pyrolyzed at 1500 °C for 1 h after being etched.

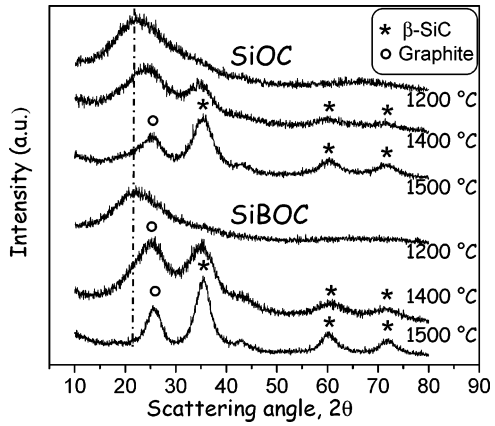

Figure 6. XRD spectra SiOC and SiBOC materials pyrolyzed at different temperatures for 1 h and then HF etched. These spectra must be compared with those obtained on the same glasses before etching (see Figure 1). The dotted line has been drawn to guide the eye and to show the consumption of the silica halo at $2\theta = 22°$.

below 5 nm while for SiBOC the pore diameter is below 10 nm with a large fraction of pores in the range 2−5 nm.

3.2.4. XRD Study. The diffraction spectra recorded on the SiOC and SiBOC glasses pyrolyzed at 1200, 1400, and 1500 °C for 1 h and then etched with HF are shown in Figure 6. The XRD patterns of the SiOC and SiBOC samples annealed at 1200 °C look similar to those recorded on the same samples before etching (cf. Figure 1): they show a completely amorphous structure with only the presence of the silica halo centered at about $2\theta = 22°$. By increasing the pyrolysis temperature, the etching of the SiO_2 and SiO_2 nB_2O_3 ($n = 1.29$) phases from the SiOC and SiBOC glasses becomes more abundant, and consequently the silica halo at $2\theta = 22°$ progressively decreases allowing the reflection associated to the crystalline phases present in these glasses (SiC and graphite) to emerge and to become, at 1500 °C, the only diffraction peaks. Indeed, at 1500 °C, the XRD spectra show only the diffraction peaks of nanocrystalline β-SiC (peaks at $2\theta = 35°$ (111), 60° (101), and 72° (211)) and of graphite (peaks at $2\theta = 26°$ (002) and 42° (101)). This result is important mainly because it allows the graphite nanocrystals to be detected and characterized because the detection and characterization of the β-SiC were already obtained from the XRD spectra of the un-etched samples (cf. Figure 1 and Table 2). Indeed, in the diffractograms recorded before etching, sp^2 C nanocrystals were only detected as a shoulder in the XRD spectrum of the SiBOC glass at 1500 °C while for the other glasses (SiOC annealed at 1400 and 1500 °C and SiBOC annealed at 1400 °C) the presence of graphite nanocrystals could not be observed.

The analysis of the line broadening, according to the Scherrer equation, performed on the (111) peak of SiC for the 1400 and 1500 °C samples and on the (002) reflection of C for the samples pyrolyzed at 1500 °C, allows us to estimate the crystal size of SiC, $D_{SiC(111)}$, and the thickness of C nanocrystallites, $L_{C(002)}$, in the direction orthogonal to the C sp^2 basal plane (Table 2). The $D_{SiC(111)}$ values compare well with those obtained for the same samples before the HF etching. Indeed, they confirm the trend of (i) increasing the crystal size with the annealing temperature and of (ii) larger β-SiC crystals for SiBOC compared to SiOC glasses.

The crystal thickness, $L_{C(002)}$, of the samples pyrolyzed at 1500 °C is larger for the SiBOC (5.3 nm) compared to that for SiOC (2.9 nm). These results agree quite well with the Raman data collected on the same samples before etching: the ordering process, as revealed by the full width at half-maximum (fwhm) of the D band at 1335 cm^{-1}, is smaller for the SiOC glass ($fwhm_{SiOC} = 87$ and 52 cm^{-1} at 1400 and 1500 °C, respectively) compared to SiBOC ($fwhm_{SiBOC} = 82$ and 42 cm^{-1} at 1400 and 1500 °C, respectively). Thus, the XRD study suggests that the presence of boron in the silicon oxycarbide network improves the ordering and the consequent growth of both β-SiC and graphite nanocrystals.

3.2.5. Raman Study. The Raman spectra of the carbon phase within the SiOC and SiBOC samples pyrolyzed at 1500 °C for 1 h after etching are reported in Figure 2. The spectra collected on the etched samples are comparable to the ones before HF attack in terms of relative intensity and width of the D and G bands. However, two main differences can be immediately appreciated: (i) the intensity of the D′ band decreased for the SiBOC glass after etching and (ii) both spectra recorded on the HF etched glasses are shifted toward lower wavenumbers. The Raman spectral parameters of the studied samples are reported in Table 3. From these data the downward shift of the Raman spectra can be estimated to be in the range 9−15 cm^{-1} for the D band and 7 cm^{-1} for the G band. The reason for the decrease of the intensity of the D′ band after etching is not clear at the moment. Conversely, the downward shift of the Raman spectra can be tentatively explained by taking into account the piezo-spectroscopic effect, which relates the vibrational frequency with the level of strain acting on the investigated phase. The etching process, by dissolving the silica and borosilicate phase, promotes a stress relaxation resulting in the observed frequency shift. Stress relaxation due to leaching phase separated glasses is a well-known phenomenon.[49] The magnitude of the stress-induced shift measured for the G band reported in the literature for amorphous carbon films is −1.9 cm^{-1}/GPa for compressive biaxial stresses.[50] Thus, the 7 cm^{-1} shift toward lower wavenumber measured in our samples for the G band suggests that the in-plane compres-

(49) Scherer, G. W.; Drexhange, M. G. *J. Am. Ceram. Soc.* **1985**, *68* (8), 419−426.
(50) Ager, J. W.; Anders, S.; Anders, A.; Brown, I. G. *Appl. Phys. Lett.* **1995**, *66* (25), 3444−3446.

sive stress acting on the carbon nanocrystals in the SiOC and SiBOC glasses is of the order of 3−4 GPa.

4. Discussion

The structure of polymer- and sol−gel-derived silicon oxycarbide glasses has been the subject of a large number of studies. The local order around the Si atoms has been investigated by ^{29}Si solid-state NMR.[22,42] At low temperature (ca. 1000−1200 °C), ^{29}Si MAS NMR indicates that Si atoms share bonds with O and C atoms in mixed silicon oxycarbide units. The distribution of the various silicon sites is, in this temperature range, completely random.[23] At higher temperature (1200−1500 °C), the redistribution reaction between Si−C and Si−O bonds leads to a phase separation between SiC_4 and SiO_4 units with a consumption of the mixed $SiO_{4-x}C_x$, $1 \leq x \leq 3$, sites.[25,51] This process results in the crystallization of nanocrystalline β-SiC, which is the only crystalline phase usually detected by XRD for these glasses.[25] The organization of the SiO_4 units is more difficult to characterize, because of the amorphous nature of the silica phase. Moreover, the presence in the SiOC glasses of excess sp^2 C layers, often called "free" C phase, has also been shown by Raman end chemical analysis.[42] Recently, Saha et al.[30] proposed a structural model for the SiOC glasses which describes these materials as composed by an open cellular structure of amorphous silica nanodomains surrounded by domain walls. The domain walls consist of graphene layers and mixed silicon oxycarbide units. This model and the existence of silica nanodomains in the silicon oxycarbide glasses is in agreement with the results of the SAXS characterization[27] and with our recent study on the etching of SiCO.[29]

For the SiBOC glasses, a previous work done in our laboratory[31] indicated that their structure and high-temperature evolution are similar to those found for SiCO. At 1200 °C the amorphous network is formed by a random mixture of silicon and boron oxycarbide units. At higher temperature, redistribution reactions between Si−O/B−O and Si−C/B−C bonds are active. However, the presence of B in the glass network accelerates the phase separation into SiC_4 and borosiloxane ($BOSi_3$) units.

In the present study a detailed characterization of the etched SiOC and SiBOC glasses has been perfomed. The experimental results will now be discussed to highlight the effect of the pyrolysis temperature and of boron on the evolution of the nanostructure, in particular with respect to the size and amount of the silica nanodomains and of the free carbon phase.

The XRD spectra collected on samples pyrolyzed at 1200, 1400, and 1500 °C before and after etching (see Figures 1 and 6) clearly indicate that the increase of the pyrolysis temperature induces the crystallization and the growth of both β-SiC and graphite nanocrystals. In the same temperature range, the redistribution reactions between Si−O/B−O and Si−C/B−C bonds[31,51] leads to the development of silica (in SiOC) and borosilicate (in SiBOC) glassy clusters whose size and amount increase with final temperature. Indeed for the SiOC glass, at 1200 °C and 1500 °C, the average pore sizes are 2.1 and 2.8 nm, respectively, and the corresponding pore volume (mesopores + micropores) is 0.205 (at 1200 °C) and 0.56 cm^3/g (at 1500 °C).

At 1200 °C, SiBOC samples cannot be etched. This result suggests that, at this temperature, the glassy borosilicate clusters are not yet formed and the amorphous network is still built up by a combination of mixed silicon oxycarbide (SiO_2C_2, $SiCO_3$) and boron oxycarbide (BOC_2, BO_2C) units, as was clearly shown in an earlier work.[31] However, above this temperature (1400 and 1500 °C), the presence of B in the silicon oxycarbide glass favors the consumption of the mixed Si (and mixed B in SiBOC) units with a phase separation into SiC_4 and borosilicate glass clusters. As shown by the XRD, larger β-SiC nanocrystals form in SiBOC glass compared to B-free SiCO samples. Moreover, N_2 adsorption characterization shows higher pore volume and larger pore size for the SiBOC compared to SiCO. At 1500 °C, the average pore sizes are 4.8 and 2.8 nm and the total pore volumes are 1.2 and 0.56 cm^3/g for SiBOC and SiOC, respectively. The composition of the borosilicate glass forming the oxide clusters can be estimated from the chemical analysis of the HF etched materials. The B/Si ratio is 0.23, which corresponds to a molar composition: SiO_2 nB_2O_3, $n = 1.29$. As revealed by the ^{11}B MAS NMR, the boron atoms remaining in the etched glass are mainly present in residual $B(OX)_3$, where X = H, Si atoms, and in boron oxycarbide sites. It is the presence, in the BO_2C and BOC_2 units, of stable B−C bonds that prevents these boron atoms to be leached out by the HF attack.

The XRD characterization of the etched samples suggests that B in SiBOC glasses, besides enhancing the SiC crystallization and the borosilicate nanocluster formation, has another quite important effect: it promotes the graphitization of nanocrystalline graphite leading to an increase of the thickness of C nanocrystallites, $L_{C(002)}$, in the direction orthogonal to the C sp^2 basal plane. $L_{C(002)}$ is 2.9 nm for SiOC and reaches 5.3 nm for SiBOC at 1500 °C. The catalytic behavior of B in promoting the graphitization of various types of nanocrystalline carbons is well-known: B-doping increases the crystallite thickness, $L_{C(002)}$, and decreases the interlayer spacing, d_{002}, of the graphite nanocrystals.[45,52−53] The detailed mechanism through which B promotes the graphitization is still not completely clear, but it has been proposed in the literature that B atoms substitute C atoms in the hexagonal graphene sheets leading to BC_3 units.[44,52] Such boron carbide units, when present in the graphene layers, act as defects and result in an enhancement of the Raman D′ band at 1617 cm^{-1}. Thus, the clear occurrence of this band in the Raman spectrum of the SiBOC sample pyrolyzed at 1500 °C can be taken as an indication of the existence of BC_3 units in the graphene layers of our SiBOC glass. This result, that is, the proposed presence of BC_3 units in the graphene layers, is not in contrast with the

(51) Burns, T.; Taylor, R. B.; Xu, Y.; Zangvil, A.; Zank, G. A. *Chem. Mater.* **1999**, *11*, 910−919.

(52) Jacques, S.; Guette, A.; Bourrat, X.; Langlais, F.; Guimon, C.; Labrugere, C. *Carbon* **1996**, *34* (9), 1135−1143.

(53) Way, B. M.; Dahn, J. R.; Tiedje, T.; Myrtle, K.; Kasray, M. *Phys. Rev. B* **1992**, *46* (3), 1697−1702.

^{11}B MAS NMR data. Indeed, even if the formation of boron oxycarbide units bearing three B−C bonds in BC_3 units has not been clearly seen, the formation of such B sites cannot be completely ruled out: BC_3 environments are indeed expected around 86 ppm.[54] If such a signal is present on the ^{11}B MAS NMR spectrum of the SiBOC sample pyrolyzed at 1500 °C (Figure 4), it would superimpose with the spinning sidebands observed in this region.

It is noteworthy that the effect of B on the graphitization of the graphene sheets of the SiBOC glass starts to be evident at temperatures as low as 1500 °C compared to 1800 °C, which is the lowest temperature at which B promotes the graphitization of different carbon materials.[45] This result seems to suggests that the insertion of B atoms in substitutional sites in the C sp^2 planes is easier for the graphene layers of SiBOC glasses compared to other forms of carbon such as mesocarbon or pyrocarbon materials. It may be due to the good dispersion of boron in the silicon boron oxycarbide network and to the fact that B−C bonds are already present at very low temperature (1200 °C).[47]

The structure of the etched SiBOC glass (at high temperature, 1400 and 1500 °C) that emerges from this study is of a highly porous material with a SSA up to 560 m^2/g, mainly formed by β-SiC and B-doped graphite nanocrystals, with residual mixed silicon and boron oxycarbide units which are most probably located at the pore surfaces. These features, and in particular the formation of B-doped carbon nanocrystals, could lead to very interesting application of these materials as carbon anode materials for Li-ion batteries.

5. Conclusions

The nanostructural evolution of polymer-derived SiOC and SiBOC glasses has been investigated in the temperature range 1200−1500 °C. The characterization has been performed using a multitechnique approach, on the as-pyrolyzed glasses and on the same samples after HF etching. The main results are as follows:

1. At low pyrolysis temperature the glasses are mainly amorphous and the nanostructure is built up by mixed silicon and boron oxycarbide units. The degree of disorder is higher for the SiBOC glasses as revealed by the fact that they cannot be etched by HF. Conversely, SiOC already at 1200 °C presents some silica clusters that can be etched out by HF producing a porous residue with a SSA of 204 m^2/g.

2. Increasing the pyrolysis temperature promotes (i) the crystallization of cubic SiC and nanocrystalline graphite and (ii) the formation of the silica-based clusters. The crystallite size of both phases increases with the temperature. As for the SiO_2 and $SiO_2-B_2O_3$ clusters, the N_2 adsorption study of the etched glasses reveals that their amount and size increase with the temperature for both compositions.

3. Chemical analysis obtained on the SiBOC glass before and after HF etching allowed the following composition of the borosilicate glass forming the oxide clusters to be estimated: $SiO_2\ nB_2O_3$, $n = 1.29$. This B/Si ratio is close to the overall B/Si ratio (0.22) for these samples.

4. By comparing the evolution of the B-free (SiOC) and B-containing samples (SiBOC), the important role of boron in promoting the nanostructural evolution has been discovered. In particular, B promotes the following:

(i) The formation of the borosilicate clusters in terms of amounts and size. Indeed, at 1500 °C the porosity and pore size revealed by the N_2 adsorption analysis are, for the SiBOC glass, both bigger compared to SiOC glass.

(ii) The graphitization of nanocrystalline sp^2 C leading to thicker graphite nanocrystals. It was worth noticing that this catalytic effect of B is active in the SiBOC samples at low temperature (1500 °C) whereas in the literature the same effect has been reported to be active, on different forms of carbon materials, starting from 1800 °C.

5. The Raman spectrum of SiBOC glasses pyrolyzed at 1500 °C shows, for the first time in silicon-based PDCs, the presence of the D′ band at 1617 cm^{-1}. This band has been considered to be the fingerprint of the substitution of some C atoms of the graphene planes with B atoms, forming BC_3 sites.

6. The downward shift of the Raman spectrum after etching suggests that the graphite nanocrystals are subjected, in the "as-pyrolyzed" state, to a compressive stress parallel to the graphene planes of the order of 3−4 GPa.

7. The highly porous SiBOC material obtained after etching, in which B-substituted graphite nanocrystals are present, could find useful applications as carbon-based materials for Li ion batteries.

Acknowledgment. This work was partly supported by the European Community FP6 through MCRTN-019601, PolyCerNet. R.P.-A. thanks the Ministerio de Educación y Ciencia from Spain for financial support under a postdoctoral fellowship. R.P.-A. and G.D.S. acknowledge the valuable discussions with Prof. Rishi Raj. G.D.S. wishes to dedicate this paper to the memory of his mother Livia De Pian who passed away on May 22nd, 2007.

CM071203Q

(54) Gervais, C.; Babonneau, F.; Ruwisch, L.; Hauser, R.; Riedel, R. *Can. J. Chem.* **2003**, *81* (11), 1359−1369.